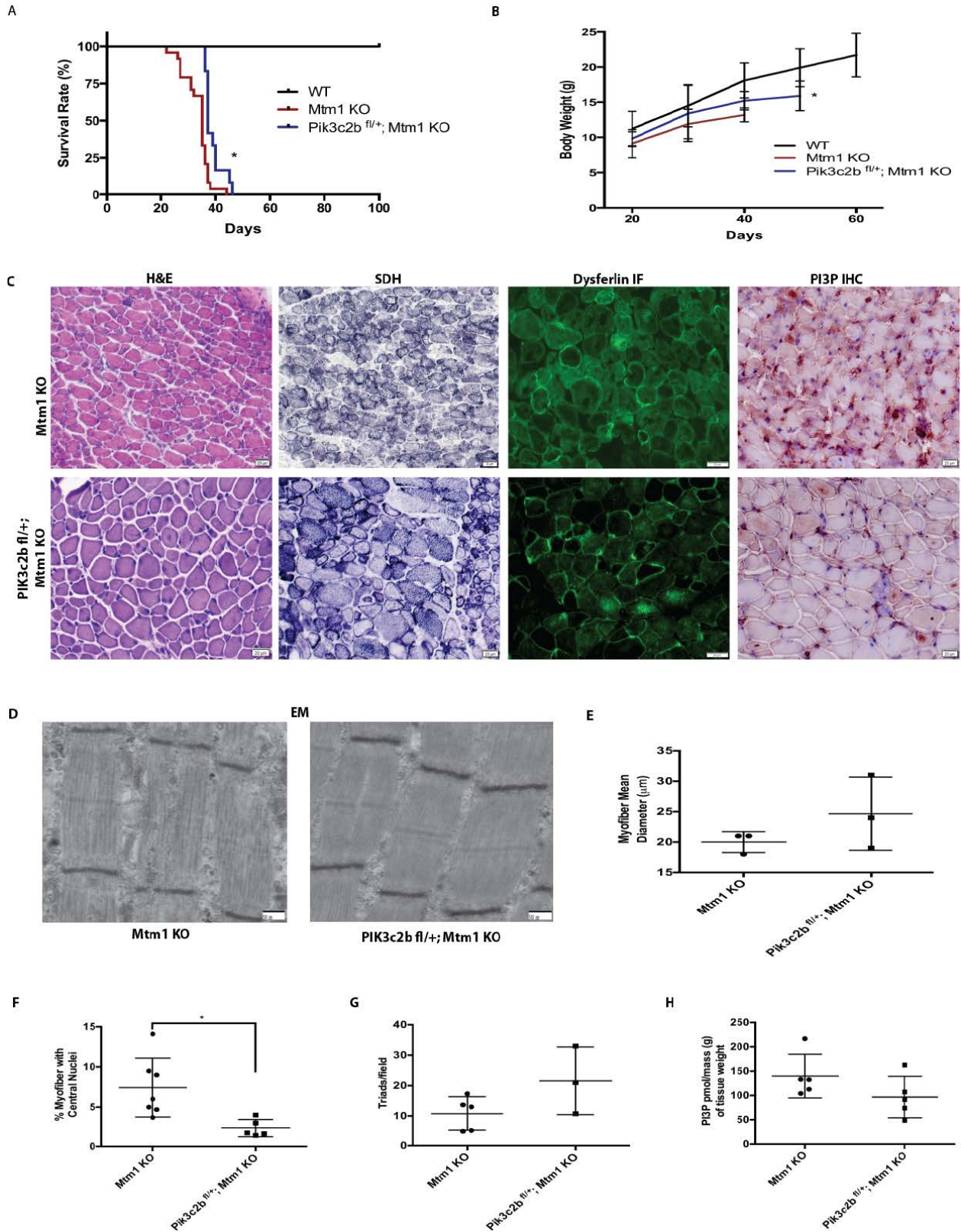


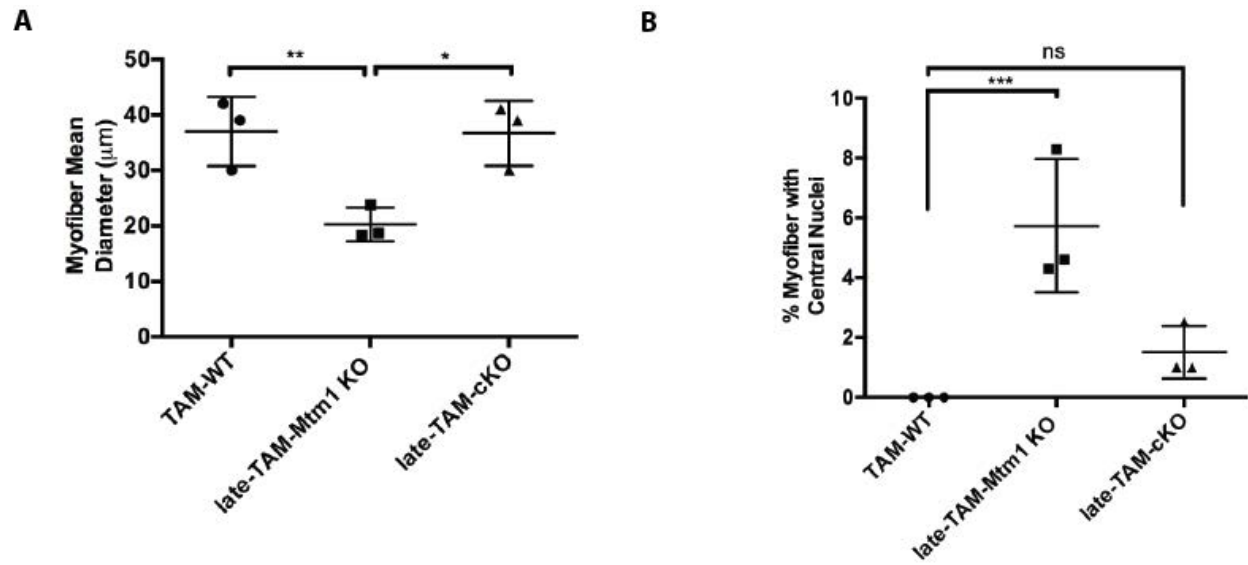
Supplementary Figure 1. Skeletal muscle specific *Pik3c2b* KO mice have normal muscle structure. **A:** Schematic of the *Pik3c2b* floxed allele with targeted disruption of the catalytic domain (exon 3-5), flanked by LoxP sites. Muscle specific *Pik3c2b* KO was generated by intercrossing floxed *Pik3c2b* (*Pik3c2b^{fl/fl}*) mice with a muscle specific Cre transgenic

[Tg(Ckmm-Cre)]. **B:** Genotyping of mice harboring homozygous floxed (f/f), heterozygous ($f/+$), or WT alleles. **C:** A significant decrease in *Pik3c2b* mRNA transcript levels in skeletal muscle as measured by qPCR (0.13 ± 0.06 fold, $n=3$) was detected in KO animals compared to WT (1.0 ± 0.05 fold, $n=3$, *** $P < 0.001$). **D:** Western blot analysis of PIK3C2B. **E:** Quantitation of PIK3C2B protein levels as determined by densitometry analysis of the western blot, using β -actin protein levels as a loading control. PIK3C2B protein levels were significantly reduced in KOs (0.14 ± 0.03 fold, $n=3$) compared to WT (1.0 ± 0.07 fold, $n=3$, *** $P < 0.001$). **F:** Photomicrographs of WT littermate and muscle-specific *Pik3c2b* KOs. *Pik3c2b* KOs at 30 days of age appear indistinguishable from WT. **G:** Motor function testing at 30 days of age using grip strength testing did not reveal any difference between *Pik3c2b* KOs (98 ± 2 %, $n=5$), and their WT littermates (100 ± 0.1 %, $n=4$). **H:** Histological analyses by light microscopy with H&E, SDH, and dysferlin immunofluorescence, and by electron microscopy, demonstrates that *Pik3c2b* KO muscle structure appears normal. In particular, there is no evidence of central nucleation, necklace fibers, or ultrastructural triad abnormalities. Scale bars = 20 μ m, EM scale bars = 500 nm. Note: WT images in H are from genotype *Tg(Ckmm-Cre)*⁺; *Pik3c2b*^{+/+}; *Mtm1*^{+/-}. Scale bar = 20 μ m, EM scale bar = 500 nm. Statistical comparisons done by unpaired students t-test.

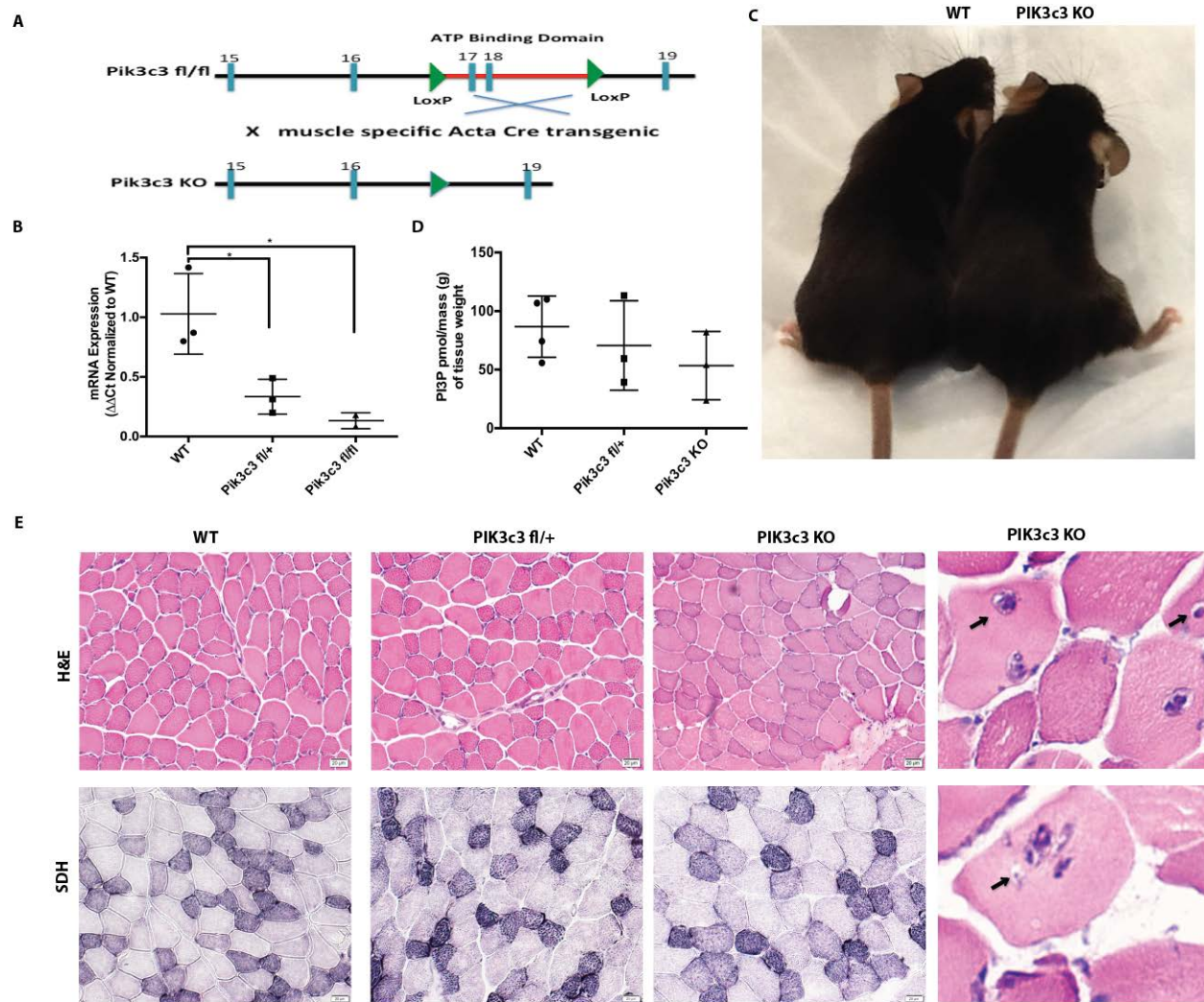


Supplementary Figure 2. Heterozygous deletion of *Pik3c2b* provides partial improvement of the *Mtm1* KO phenotype. A: Heterozygous deletion of *Pik3c2b* improves survival of *Mtm1*

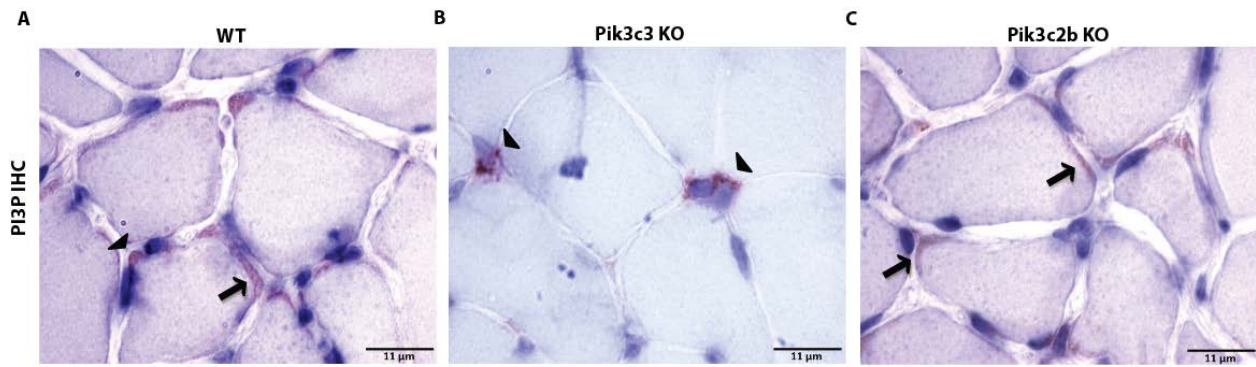
KO. *Pik3c2b*^{fl/+}; *Mtm1* KOs (n=11) have a median survival of 37 days compared to 35 days for *Mtm1* KOs (n=24, * P < 0.05). **B**: Body weight of *Pik3c2b*^{fl/+}; *Mtm1* KOs (n=11), *Mtm1* KOs (n=24), and WT (n=12). *Pik3c2b*^{fl/+}; *Mtm1* KOs showed a small but significant improvement in body weight vs. *Mtm1* KO alone (* P < 0.05). **C**: Histopathological assessment reveals that *Pik3c2b*^{fl/+}/*Mtm1* KO muscle has increased myofiber size, decreased central nuclei number, and intermediate restoration of PI3P levels. Scale bars = 20 μ m **D**: *Pik3c2b*^{fl/+}; *Mtm1* KOs have similar triad appearance as compared to *Mtm1* KOs (scale bars = 500 nm). **E**: *Pik3c2b*^{fl/+}; *Mtm1* KOs have an intermediate restoration in myofiber size. The average myofiber diameter for *Pik3c2b*^{fl/+}; *Mtm1* KOs was 25 \pm 3.4 μ m (n=3) vs. 20 \pm 1 in *Mtm1* KOs (n=3, P = 0.15). **F**: *Pik3c2b*^{fl/+}; *Mtm1* KOs have a significant decrease in fibers with central nuclei (2.8 \pm 0.9 %, n=4) when compared to *Mtm1* KOs (6.3 \pm 0.9 %, n=6) (* P < 0.05). **G**: Ultrastructural analysis and quantification of triad number. There is a non-significant trend toward increased triad number in *Pik3c2b*^{fl/+}; *Mtm1* KOs [21 \pm 6.4 triads/field (n=3) vs. 11 \pm 2.5 triads/field for *Mtm1* KOs (n=5), P = 0.10). **H**: PI3P levels are partially but not statistically significantly restored in the *Pik3c2b*^{fl/+}; *Mtm1* KOs, as determined by PI(3)P ELISA. PI3P levels were 97 \pm 19 pmol/mass g for *Pik3c2b*^{fl/+}; *Mtm1* KOs (n=5), compared to 140 \pm 20 pmol/mass g for *Mtm1* KOs (n=5) (p = 0.15). [note: *Mtm1* KO light microscopy (D) is from genotype *TgCkmm-Cre*⁻; *Pik3c2b*^{fl/+}; *Mtm1*^{-y} and electron microscopy (E) is from *TgCkmm-Cre*⁺; *Pik3c2*^{+/+}; *Mtm1*^{-y}]. Statistical comparisons done by one-way ANOVA followed by Dunnett's multi-comparisons test.



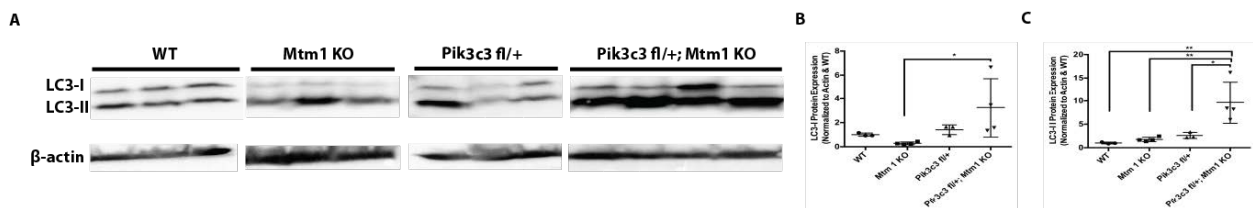
Supplementary Figure 3. Temporal knockout in *Mtm1* KOs of *Pik3c2b* after symptom onset restores myofiber size and reduces central nuclei. **A:** Late-TAM-cKO [i.e. *Pik3c2b*^{fl/fl}; *Mtm1* KO; Tg(ER-Cre) with TAM treatment initiated at 30 days for one week] have restored myofiber size. Average myofiber diameters were: 37 \pm 6.2 μm for TAM-WT (n= 3), 20 \pm 3.1 μm for late-TAM-*Mtm1* KO (n=3, **P = 0.01 when compared to WT), and 37 \pm 5 μm for late-TAM-cKO (n=3, * P = 0.01 when compared to late-TAM-*Mtm1* and P = 0.79 when compared to WT). **B:** Comparison of percent myofibers with central nuclei reveals a significant decrease in the late-TAM-cKO. The average percent of central nuclei for WT (n=3) was 0.0 %, for *Mtm1* KO was 5.7 \pm 2.2 % (n=3, *** P = 0.005 when compared to WT), and for late-TAM-cKO was 1.5 \pm 0.7 (n=3, **P = 0.01 when compared to *Mtm1* KO and P = 0.48 as compared to WT). Statistical comparisons done by one-way ANOVA followed by Dunnett's multiple comparisons test.



Supplementary Figure 4. Skeletal muscle specific *Pik3c3* KO are healthy but manifest mild myopathic abnormalities **A:** Schematic of the *Pik3c3* floxed allele with loxP sites that flank exons 17 and 18 (containing the ATP Binding domain). Skeletal muscle specific *Pik3c3* KO were generated by intercrossing *Pik3c3*^{fl/fl} mice with a skeletal muscle specific Acta-Cre transgenic line. **B:** Muscle specific KO of *Pik3c3* results in a significant reduction in *Pik3c3* mRNA transcript levels as measured by qPCR (*Pik3c3*^{fl/fl} = 13 ± 0.1 fold, n=3, * P < 0.05) (*Pik3c3*^{fl/+} = 0.3 ± 0.1 fold change, n=3, * P < 0.05) (WT = 1.0 ± 0.1 folds, n=3). **C:** Photomicrographs of littermates at age 30 days. Muscle-specific *Pik3c3* KO animals appear to be indistinguishable in appearance from their wild type littermates. **D:** Total PI3P levels are decreased in the *Pik3c3* KO skeletal muscle, as determined using a PI3P mass ELISA [purified lipid (pmol)/mass (g) of muscle tissue, with *Pik3c3* KO = 53.4 ± 24 pmol/mass g (n=3), *Pik3c3* fl/+ = 71 ± 31 pmol/mass g (n=3) and WT = 86.7 ± 22 pmol/mass g (n=4). This decrease did not, however, reach statistical significance (comparison done by ANOVA followed by Dunnett's multi-comparison test). **E:** Histological analysis by H&E and SDH staining reveals myopathic changes in *Pik3c3* KO muscle. We observed a small increase in internalized nuclei, increased fiber size variability, and several fibers with vacuoles, all consistent with changes we previously described and with the alterations seen in a vacuolar myopathy. (scale bar = 20 μm)

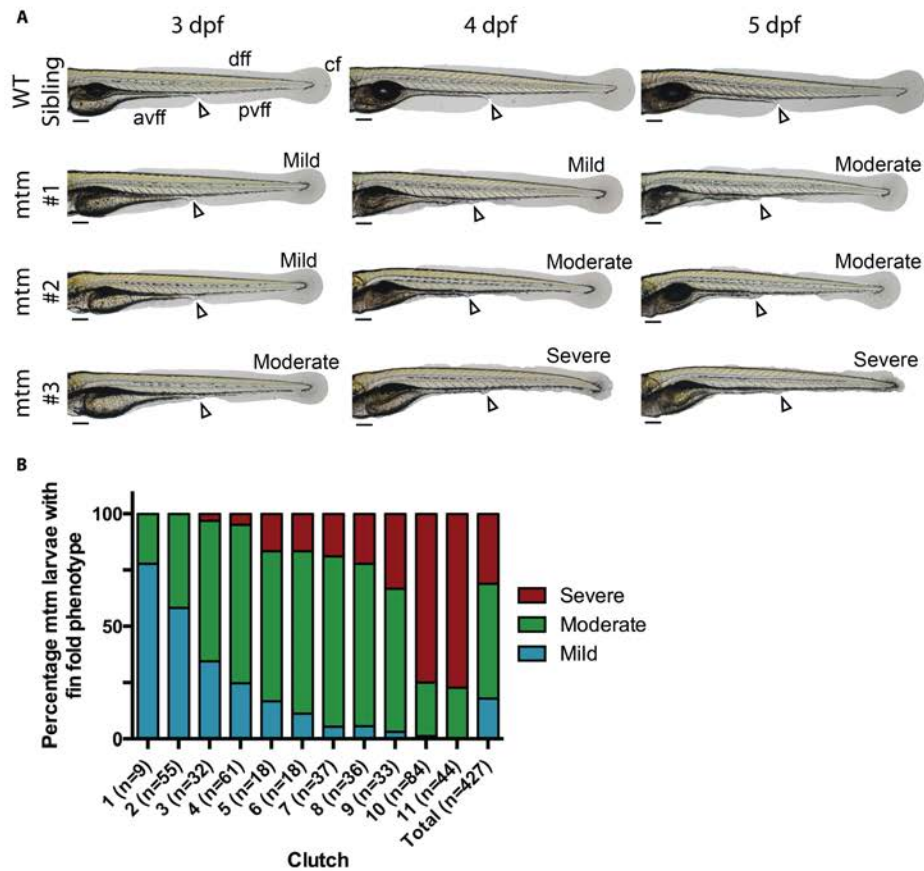


Supplementary Figure 5: Individual kinase knockouts result in differential changes in PI3P distribution. PI3P subcellular localization as determined by immunohistochemistry on cross section of TA muscle. In wild type (WT) muscle fibers, the distribution of PI3P was seen along the sarcolemmal membrane (arrow) as well as in the perinuclear compartment (arrow head). In *Pik3c3* KO muscle PI3P staining is restricted to the perinuclear compartment (arrowhead), implying that PIK3C3 is responsible for producing the sarcolemmal PI3P. Conversely, in *Pik3c2b* KO muscle the PI3P staining is found along the sarcolemmal membrane (arrow), indicating that PIK3C2B regulates perinuclear PI3P production. (scale bar = 11 μ m)

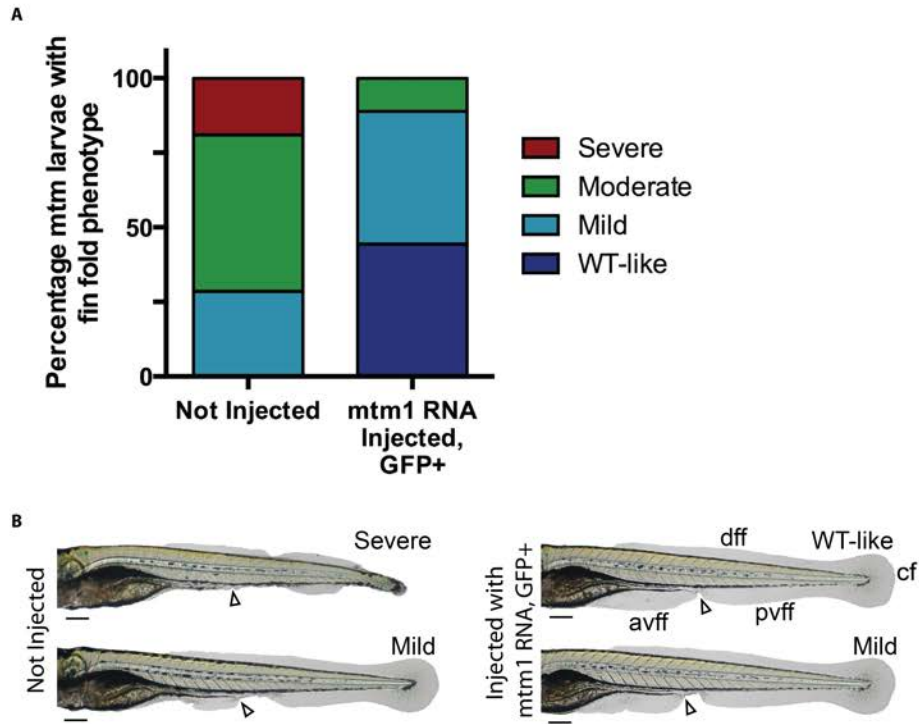


Supplementary Figure 6: Aberrant autophagy in *Pik3c3*^{+/-};*Mtm1*^{-y} skeletal muscle.

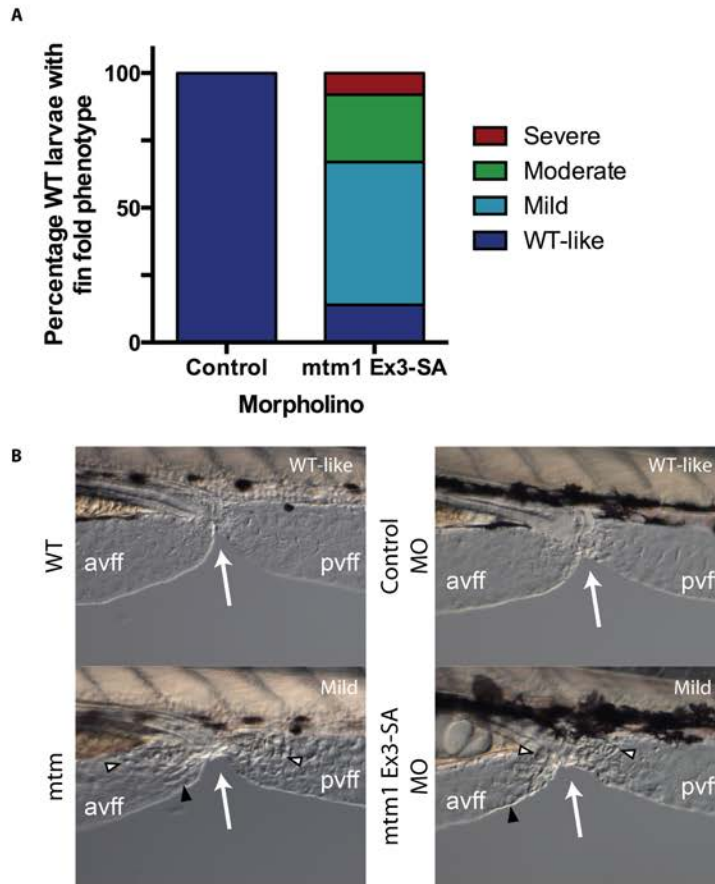
A: Western blot analysis of LC3 and β -actin on protein extracts from quadriceps muscle. **B:** Quantitation of LC3-I protein levels as determined by densitometry analysis of the western blot, using β -actin protein levels as a loading control. Significant increase of LC3-I protein levels in *Pik3c3*^{fl/+};*Mtm1* KOs (3.3 \pm 0.96 folds, n=4) as compared to *Mtm1* KO (0.28 \pm 0.05 folds, n=3, * P < 0.05). **C:** Quantitation of LC3-II protein levels reveal significant increase of LC3-II protein levels in *Pik3c3*^{fl/+};*Mtm1* KOs (9.7 \pm 1.8 folds, n=4) as compared to *Mtm1* KO (1.8 \pm 0.4 folds, n=3, ** P < 0.01) or *Pik3c3*^{fl/+} alone (2.6 \pm 0.8 folds, n=3, * P < 0.05) or WT (1 \pm 0.02, n=3, ** P < 0.01). Comparisons done by one-way ANOVA followed by Dunnett's multi-comparison test.



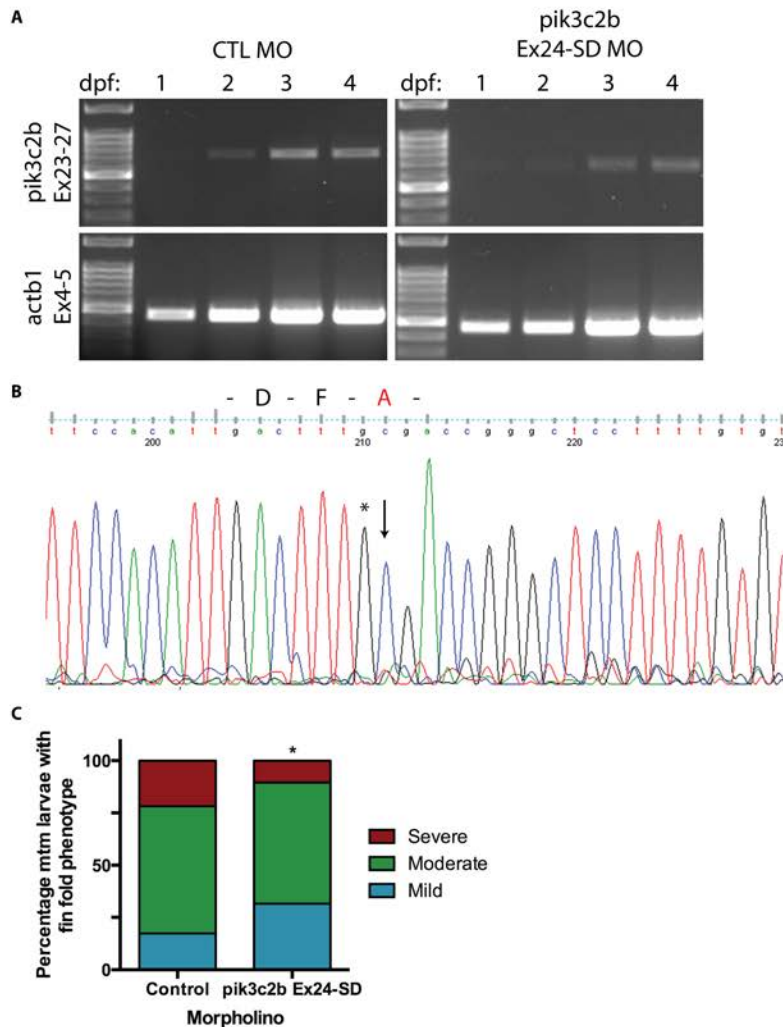
Supplementary Figure 7. Fin fold degeneration of the *mtm* mutant phenotype is progressive and severity varies between individuals. **A:** Bright-field images tracking the fin morphology of individual WT and *mtm* larvae from 3 dpf to 5 dpf (scale bar = 200 μ m). As shown, *mtm* fin folds progressively degenerate and the extent of degeneration is variable between individuals. The severity of fin degeneration is given an ordinal score from "mild" to "severe" depending on the degree of fin loss. A mild phenotype is scored when the avff and pvff are incompletely lost on either side of the presumptive cloaca (white arrowhead) while the cf and dff remain intact. Moderate is defined as the complete loss of the avff and partial loss of the pvff while the cf and dff remain intact. Severe mutants have lost the avff, pvff, and significant portions of the cf and dff. **B:** The severity of *mtm* mutants is variable between different clutches, i.e. different parents. The clutch-to-clutch variability called for a method of separating mutants into different groups (i.e. for chemical screens) such that their phenotypic distributions were similar. This experimental setup is described in the Materials and Methods section. Abbreviations: avff=anterior ventral fin fold; pvff=posterior ventral fin fold; dff=dorsal fin fold; cf=caudal fin.



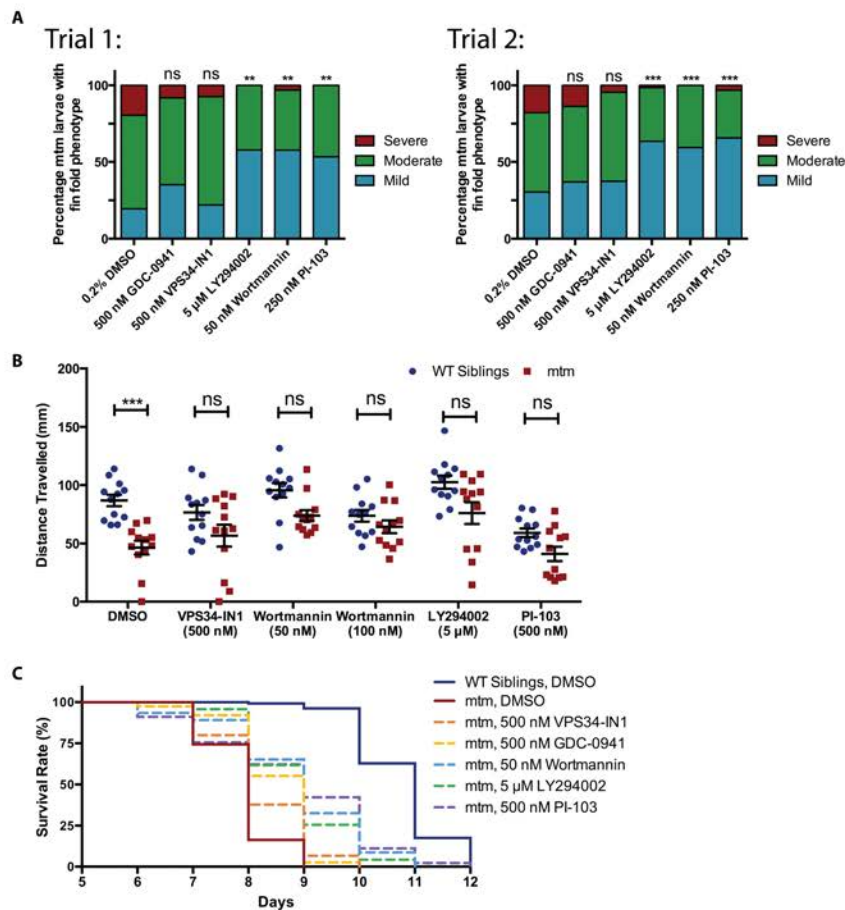
Supplementary Figure 8. Expression of *mtm1+::EGFP* RNA prevents or ameliorates fin degeneration in *mtm* mutants at 4 dpf. **A:** Proportions of *mtm* larvae with a fin fold phenotype. The majority of mutants that were not injected ($n=21$) had moderate to severe fin degeneration where the avff is lost and significant portions of the pvff, cf, and df are lost. In contrast, the majority of *mtm* mutants injected with *mtm1::EGFP* RNA had WT-like or mild fin phenotypes where the fin folds remain intact. **B:** Representative bright-field images of genotyped *mtm* mutants from each group showing their phenotype (white arrowhead indicates the cloaca; scale bar = 200 μ m). Note that mild mutants that were not injected often had partial loss of the avff. Abbreviations: avff=anterior ventral fin fold; pvff=posterior ventral fin fold; dff=dorsal fin fold; cf=caudal fin.



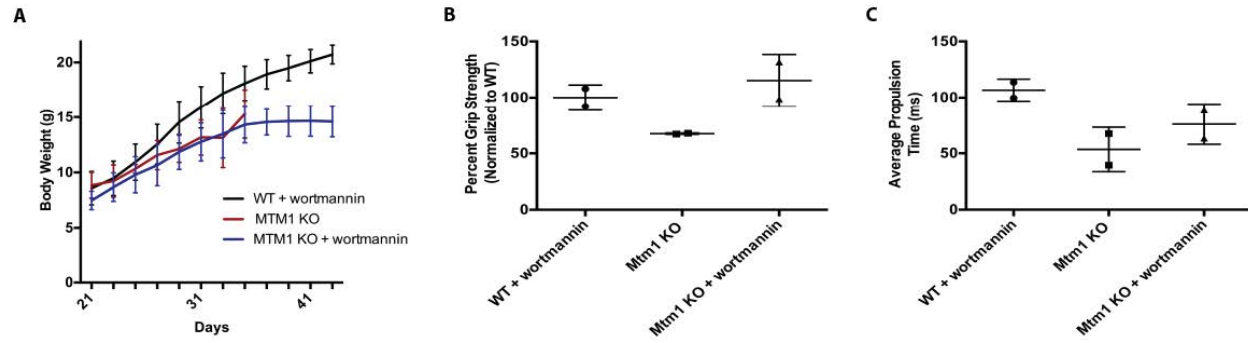
Supplementary Figure 9. Morpholino knockdown of *mtm1* phenocopies the fin fold degeneration seen in *mtm* mutants. **A:** Proportions of WT larvae with a fin fold phenotype at 4 dpf after injection with 7.5 ng of either control ($n=40$) or *mtm1* exon 3-splice acceptor (Ex3-SA; $n=100$) morpholino. **B:** DIC images focused near the presumptive cloaca (white arrow) at 3 dpf show that *mtm* mutants and *mtm1* morphants have similar morphology at the beginning of ventral fin fold degeneration. Both mutant and morphant fins have visible clusters (white arrowheads) and depressions (black arrowheads). Note: DIC images were taken at the same magnification. Abbreviations: avff=anterior ventral fin fold; pvff=posterior ventral fin fold.



Supplementary Figure 10. Morpholino knockdown of *pik3c2b* lessens the severity of *mtm* fin fold degeneration. **A:** RT-PCR of embryos shows that *pik3c2b* transcripts are qualitatively less abundant between 2 and 4 dpf after injection with *pik3c2b* Ex24-SD MO compared to CTL MO. **B:** Sanger sequencing of an RT-PCR fragment from 2 dpf embryos injected with *pik3c2b* Ex24-SD MO show that it results in the mis-splicing of 43 bp from exon 24, producing a frameshift, a premature stop codon, and mutation of the conserved ATP-coordinating DFG motif (amino acid change shown above chromatogram). Asterisk indicates the end of normal exon 24 sequence, which at that point has been mis-spliced and is now continuous with the start of exon 25 (black arrow). **C:** Knockdown of *pik3c2b* significantly lessens the severity of fin fold degeneration in 4 dpf *mtm* mutants ($*P < 0.0403$). Control MO, $n=46$; *pik3c2b* MO, $n=38$; Kruskal-Wallis test, followed by Mann-Whitney U test.



Supplementary Figure 11. Treatment of *mtm* larvae with pan-PI3K inhibitors improves various aspects of the phenotype. **A:** Severity of fin fold phenotype in 4 dpf *mtm* mutants is significantly improved after treatment with 100 nM PI-103 (** $P < 0.0051$) and 10 μ M LY294002 (** $P < 0.0033$). Treatment with 5 μ M LY294002, or 50-100 nM wortmannin tends to lessen the severity of the *mtm* phenotype, consistent with data presented in Figure 7. Again, there is no obvious change in the phenotypic distribution by inhibiting class III PI3K VPS34. At 5 dpf, when fin degeneration progresses, we still see a trend towards lesser severity in *mtm* mutants treated with LY294002, wortmannin (** $P < 0.0008$) and PI-103. From left-right: (4 dpf) $n=41, 43, 48, 43, 37, 40, 44$; (5 dpf) $n=43, 45, 38, 47, 46, 44$. Kruskal-Wallis test, followed by Dunn's post-test. **B:** Motor behaviour assay showing the effect of various chemicals treatments. While untreated mutants travel roughly half the distance of their WT siblings, treatment with PI3K inhibitors bridges the gap between mutants and their siblings suggesting the chemical effect of PI3K inhibition is *mtm*-specific. Error bars represent SEM. $n=12$ each group. **C:** VPS34-IN1 and GDC-0941 have a modestly positive effect on survival based on the slope of the curve and maximum survival.). Legend top-bottom: $n=132, 45, 38, 43, 46, 47, 44$.



Supplementary Figure 12. Restoration of grip strength and treadmill performance but not body weight in wortmannin treated *Mtm1* KOs. **A:** Plot of body weight versus postnatal age for WT + wortmannin, *Mtm1* KO without treatment, and *Mtm1* KO + wortmannin. *Mtm1* KO mice treated with wortmannin (n = 5) have a similar body weight to untreated *Mtm1* KOs (n=4). **B:** *Mtm1* KO treated with wortmannin have restored muscle power at 32 days of age, with mean grip strength of 115 ± 16 % (n=2) compared to 67 ± 1 % in the *Mtm1* KO alone (n=2) and 100 ± 8 % (n=2) in WT + wortmannin. **C:** *Mtm1* KOs treated with wortmannin have a modest improvement in motor function, as measured by treadmill analysis. The average propulsion time measurement at 32 days of age for *Mtm1* KO + wortmannin was 76 ± 12 ms (n=2), for *Mtm1* KO + DMSO was 53 ± 13 ms (n=2), and WT + wortmannin was 107 ± 7 ms (n=2).

Supplementary Table I: Mouse strains and genetic backgrounds

| Strain | Parent strain background | Jackson lab stock # | Notes |
|----------|---|---------------------|---|
| Mtm1 | C57BL/6 | N/A | Reference: Buj-Bello <i>et al.</i> (2002) <i>Proc. Natl. Acad. Sci.</i> |
| Mck-Cre | mixed C57BL/6J ; C57BL/6N genetic background. | 6475 | backcrossed > 10 generations to C57BL/6 |
| Acta-Cre | (C57BL/6J x SJL)F1 | 6139 | backcrossed > 10 generations to C57BL/7 |
| Pik3c2b | 129X1/SvJ x 129S1/Sv)F1 | 5702 | backcrossed > 10 generations to C57BL/6 |
| Pik3c3 | C57BL/6N | 19081 | backcrossed > 10 generations to C57BL/8 |
| Cre-ER | C57BL/6 | 8463 | backcrossed > 10 generations to C57BL/9 |

Supplementary Table II: Demographics of mice analyzed (numbers and background strains). The background of each mouse line is given (see also Supplementary Table I), along with the numbers analyzed. This table confirms that *Mtm1* KO mice have uniform mortality regardless of the background strain, and that the changes in survival noted with *Pik3c2b* KO were associated only with *Pik3c2b* deletion. Note that in several experiments, animals were terminated at 100 days for comprehensive analyses of their muscle phenotype(s).

| Mck; Pik3c2b; MTM1 | | | |
|------------------------------------|---|--------------------|-----------------------|
| Strain | Genotype of offspring (Mck-Cre; Pik3c2b; MTM1) | # analyzed | Survival (dys) |
| WT | +; +/+; +/Y | 7 | 300 |
| | -; +/+; +/Y | 4 | 300 |
| | -; F/+; +/Y | 5 | 300 |
| | -; F/F; +/Y | 4 | 300 |
| Mtm1 KO | +; +/+; -/Y | 10 | 35 |
| | -; +/+; -/Y | 7 | 36 |
| | -; F/+; -/Y | 7 | 35 |
| | -; F/F; -/Y | 5 | 37 |
| dKO | +; F/F; -/Y | 18 | 300 |
| Pik3c2b KO | +; F/F; +/Y | 12 | 300 |
| Cre-ER; Pik3c2b; MTM1 (cKO) | | | |
| Strain | Genotype of offspring (ER-Cre; Pik3c2b; MTM1) | n# analyzed | Survival (dys) |
| Mtm1 KO | (het; +/+; -/Y) | 2 | 34 |
| | (-; F/F; -/Y) | 1 | 38 |
| | (-; F/+; -/Y) | 1 | 36 |
| cKO | (het; F/F; -/Y) | 10 | 93 |
| Acta; Pik3c3; MTM1 | | | |
| Strain | Genotype of offspring (Acta-Cre; Pik3c3; MTM1) | n# analyzed | Survival (dys) |
| WT | +; +/+; +/Y | 4 | 100 |
| | -; +/+; +/Y | 3 | 100 |
| | -; F/+; +/Y | 3 | 100 |
| | -; F/F; +/Y | 1 | 100 |
| Mtm1 KO | +; +/+; -/Y | 3 | 33 |
| | -; +/+; -/Y | 2 | 34 |
| | -; F/+; -/Y | 3 | 37 |
| | -; F/F; -/Y | 2 | 34 |
| Pik3c3 KO | +; F/F; +/Y | 5 | 100 |
| Pik3c3 Fl/+; Mtm1 KO | +; F/+; -/Y | 5 | 29 |

Supplementary Table III. *In vitro* IC₅₀ values (μM) for PI3K inhibitors against phosphoinositide kinases. Data compiled from multiple sources.

| Chemical | Concentrations Used in this Study (μM) | Class I PI3Ks* (p110α, p110β, p110γ, p110δ) | PIK3C2 α (Class II PI3K) | PIK3C2 β (Class II PI3K) | VPS34 (Class III PI3K) | PI4Ks |
|------------|--|---|---|---|--------------------------|--|
| LY294002 | 5, 10 | 1-50 ^{1†} 2.9-38 ² 0.6 ³ 1.2 ⁴ | 100 ^{1†} >100 ² 27.3 ³ | 1-10 ^{1†} 5.7 ² 10.4 ³ 6.9 ⁴ | 3.49 ³ | >100 ^{1†} >100 ² >100 ³ |
| Wortmannin | 0.05, 0.1 | 0.001-0.01 ^{1†,4} | 0.5 ^{1†} | 0.001-0.01 ^{1†,4} | 0.001-0.01 ^{1†} | 0.1 ^{1†} |
| PI-103 | 0.1, 0.5 | 0.008-0.15 ¹ | ~1 ¹ | 0.026 ¹ | 2.3 ¹ | 50-100 ¹ |
| GDC-0941 | 0.1, 0.5 | 0.007-0.224 ³ | >100 ³ | 0.59 ³ | >100 ³ | >100 ³ |
| VPS34-IN1 | 0.1, 0.5 | 1.896-21.44 ⁵ | >10 ⁵ | >10 ⁵ | 0.025-0.076 ⁵ | >10 ⁵ |

*Single values represent IC₅₀ of p110α catalytic subunit. Otherwise, the range of IC₅₀ values for all four isoforms is shown.

[†]Exact values were not reported.

References

1. Knight, Z.A. et al. A Pharmacological Map of the PI3-K Family Defines a Role for p110a in Insulin Signaling. *Cell*, **125**, 733-747 (2006).
2. Knight, Z.A. et al. Isoform-specific phosphoinositide 3-kinase inhibitors from an arylmorpholine scaffold. *Bioorganic and Medicinal Chemistry*, **12**, 4749-4759 (2004).
3. Kong, D. et al. Inhibition profiles of phosphatidylinositol 3-kinase inhibitors against PI3K superfamily and human cancer cell line panel JFCR39. *European Journal of Cancer*, **46**, 1111-1121 (2010).
4. Arcaro, A. et al. Human Phosphoinositide 3-Kinase C2b, the Role of Calcium and the C2 Domain in Enzyme Activity. *The Journal of Biological Chemistry*, **273**, 33082-33090 (1998).
5. Bago, R. et al. Characterization of VPS34-IN1, a selective inhibitor of Vps34, reveals that the phosphatidylinositol 3-phosphate-binding SGK3 protein kinase is a downstream target of class III phosphoinositide 3-kinase. *Biochem. J.*, **463**, 413-427 (2015).